Elemental x-ray imaging using Zernike phase contrast*

Qi-Gang Shao(邵其刚)[1], Jian Chen(陈健)[1], Faiz Wali[1], Yuan Bao(鲍园)[1], Zhi-Li Wang(王志立)[2], Pei-Ping Zhu(朱佩平)[3,†], Yang-Chao Tian(田扬超)[1,‡], and Kun Gao(高昆)[1,¶]

[1] *National Synchrotron Radiation Laboratory, University of Science and Technology of China, Hefei* 230029, *China*
[2] *School of Electronic Science and Applied Physics, Hefei University of Technology, Hefei* 230009, *China*
[3] *Institute of High Energy Physics, Chinese Academy of Science, Beijing* 100049, *China*

(Received 13 April 2016; revised manuscript received 17 May 2016; published online 25 August 2016)

We develop an element-specific x-ray microscopy method by using Zernike phase contrast imaging near absorption edges, where a real part of refractive index changes abruptly. In this method two phase contrast images are subtracted to obtain the target element: one is at the absorption edge of the target element and the other is near the absorption edge. The x-ray exposure required by this method is expected to be significantly lower than that of conventional absorption-based x-ray elemental imaging methods. Numerical calculations confirm the advantages of this highly efficient imaging method.

Keywords: x-ray imaging, Zernike phase contrast, elemental imaging

PACS: 87.59.–e, 68.37.Yz, 87.64.mh **DOI:** 10.1088/1674-1056/25/10/108702

1. Introduction

X-rays have been employed as a quantitative mapping tool of elemental constituents since the last century.[1,2] At the absorption edge of an element, the complex x-ray atomic scattering factor experiences rapid and substantial change.[3,4] This elemental specific change has been exploited using x-ray absorption contrast imaging technique to obtain element specific image.[5–9] The technique typically requires two x-ray images: one is at x-ray energy slightly below the absorption edge energy and the other is at x-ray energy slightly above the absorption edge energy. After proper normalization of the two images in intensity, subtraction of the normalized images will yield an image of the target element. This elemental imaging technique is simple, straight forward, and fast, especially when a synchrotron x-ray source is used.[10–13]

For high Z elements, however, the change of the real part of their atomic scattering factors across an absorption edge between 0.3 keV–2 keV can be larger than that of the corresponding imaginary part,[3,4] and we refer to the change as resonance peak. Figure 1 shows the components of the refractive index of four elements each as a function of x-ray energy.[4] Here, we underline that for each element, the change of the real part across an absorption edge is larger than that of the imaginary part. Effective use of the large change in the real part of the atomic scattering factor may therefore offer significant advantage in terms of elemental sensitivity, yield, and radiation dose.

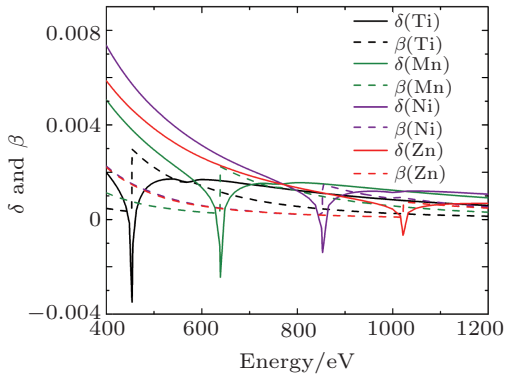


Fig. 1. (color online) Plots of refractive-index decrement δ and imaginary part β of the refractive index versus energy for different metals (black for Ti, green for Mn, purple for Ni, and red for Zn). Curves are based on Ref. [4].

Here, we propose a new elemental imaging method by using Zernike phase contrast (the changes of both the real and the imaginary parts of the atomic scattering factor) instead of absorption contrast (solely the change of the imaginary part). In our proposed method, two phase-contrast images are collected by using Zernike phase contrast setup: one is at energy corresponding to the resonance peak and the other is close to the resonance peak. The two images are normalized and subtracted to obtain an image of the target element. Our proposed method can be readily performed on existing Zernike phase contrast x-ray microscopes that are available by using synchrotron and laboratory x-ray sources. In Zernike phase contrast x-ray microscopes, the sample is placed on the focus of the condenser, a zone plate is used as an objective, and a phase ring is placed in the back focal plane of the zone plate to achieve $\pi/2$ or $3\pi/2$ phase shift.[14–17] Only the working

*Project supported by the National Basic Research Program of China (Grant No. 2012CB825801) and the National Natural Science Foundation of China (Grant Nos. 11505188, and 11305173).

†Corresponding author. E-mail: zhupp@ihep.ac.cn
‡Corresponding author. E-mail: ychtian@ustc.edu.cn
¶Corresponding author. E-mail: gaokun@ustc.edu.cn

© 2016 Chinese Physical Society and IOP Publishing Ltd

energy needs to be changed once in the system to perform the new elemental imaging experiment. Possible problems, such as different magnifications of the images at different energies, in the experiment could be solved just as in the absorption based method.[18]

2. Simulation and calculation

To demonstrate the effect of the proposed method, we simulate the imaging procedure of different metal particles within a model cell as illustrated in Fig. 2(a). The cell contains zinc (Zn) and gold (Au) nanoparticles each with a 20-nm diameter. The cell contains 80% water and 20% organic material with a composition of $C_{22}H_{10}N_2O_5$, and has an average density $\rho_c = 1.43$ g/cm^3.[19] To test the element-sensitivity a protein cluster is placed near these particles. For the model protein structure we use the stoichiometric composition $H_{48.6}C_{32.9}N_{8.9}O_{8.9}S_{0.3}$ with the density $\rho_p = 1.35$ g/cm^3.[20] In the simulation, the setup is the same as that used in conventional Zernike phase contrast microscope.[14–17] The resolution of the microscope is 20 nm, a gold-made phase ring is used, and the radius and width of phase ring are selected according to the condenser properties. Poisson noise is added to simulate the physical noise of x-ray photons. Since the phase shift of Zn changes dramatically near the resonance peak around 1022.3 eV,[3] we choose a suitable pair of energies, i.e., 1022.3 eV and 973.7 eV, as working energies. For comparison, we also calculate the required exposure of absorption methods. In the absorption method the working energies are 1022.3 eV and 1012.4 eV. Figures 2(b)–2(d) show the simulation results of regular absorption transmission x-ray microscopy (TXM) images (Figs. 2(b) and 2(c)) and phase contrast image (Fig. 2(d)), in which Zn and Au particles are not clearly distinguished from each other. Figure 3 shows images after the subtraction by using the phase contrast data (Fig. 2(a)) and the absorption data (Figs. 2(b)–2(f)), respectively. In subtraction images Zn nanoparticles stand out, while Au nanoparticles and the protein cluster disappear. In addition, we calculate the signal-to-noise ratios (SNRs) for the three Zn nanoparticles in Fig. 3 under different photon number densities (PNDs). The signal is an average value of 9×9 pixels (the size of nanoparticles) and the noise is calculated by the standard deviation of the same size of background area. The data show that to achieve the same picture quality, the required exposure in phase contrast is only about one-third that required in the absorption method.

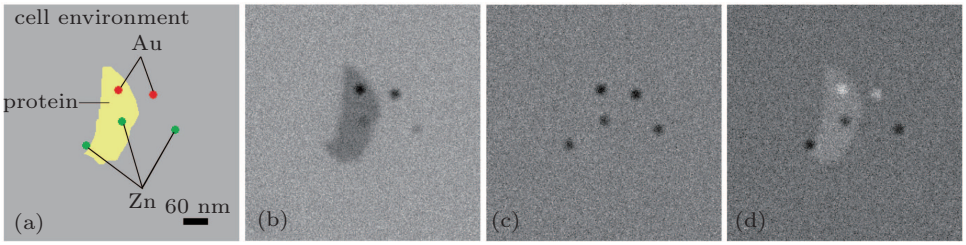


Fig. 2. (color online) (a) Profile of the sample, with the bulk protein and Zn and Au nanoparticles inside a cell; (b) absorption TXM image in the water window; (c) absorption TXM image at the energy E_1 (1022.3 eV); (d) x-ray phase contrast image at the energy E_1 (1022.3 eV). All images have PND $= 4 \times 10^{10}$ photons/μm^2.

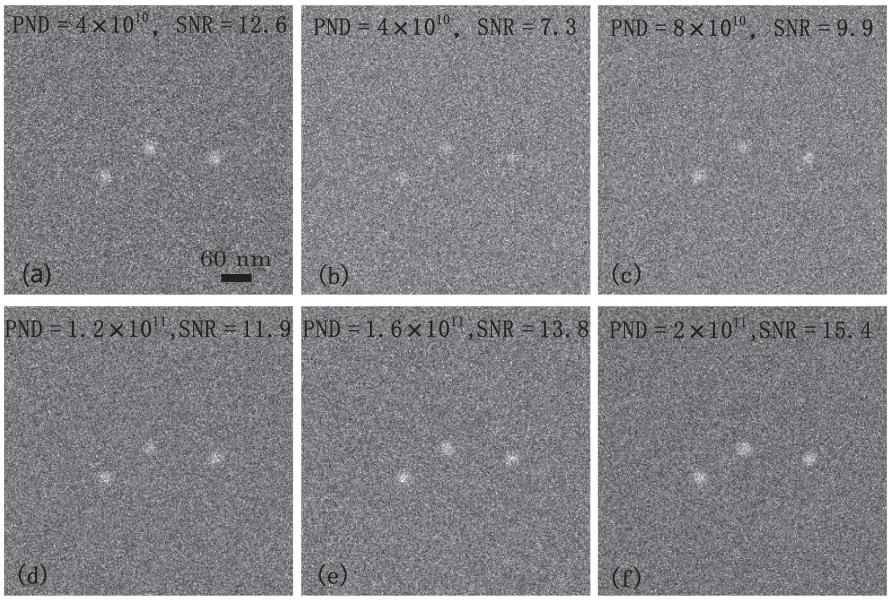


Fig. 3. Subtraction images: (a) phase contrast, and (b)–(f) absorption contrasts. The sample exposures correspond to PND: 4×10^{10}, 4×10^{10}, 8×10^{10}, 1.2×10^{11}, 1.6×10^{11}, 2×10^{11} photons/μm^2, respectively. The SNRs of the images are 12.6, 7.3, 9.9, 11.9, 13.8, and 15.4, respectively.

For in-depth analysis and quantifying the advantages of elemental imaging with using the phase contrast, we consider PND to achieve given SNR, as a criterion. The PND for conventional TXM images is calculated by[15]

$$\mathrm{PND}^0 = \frac{\mathrm{SNR}^2}{F\eta_{\mathrm{zp}}}\frac{I_\mathrm{s}+I_\mathrm{b}}{(I_\mathrm{s}-I_\mathrm{b})^2}, \tag{1}$$

where I_s and I_b are the intensities of sample and background respectively, F is the area of the target feature, and η_{zp} is the first order efficiency of zone plate. Similarly, PND for the new elemental imaging method can be calculated as

$$\mathrm{PND} = (1+K)\frac{\mathrm{SNR}^2\,[K(I_{\mathrm{s}1}+I_{\mathrm{b}1})+(I_{\mathrm{s}2}+I_{\mathrm{b}2})]}{F\eta_{\mathrm{zp}}(KI_{\mathrm{s}1}-I_{\mathrm{s}2})^2}, \tag{2}$$

where $K = I_{\mathrm{b}2}/I_{\mathrm{b}1}$ is the background normalization factor, and parameters with subscripts 1, 2 indicate parameters at corresponding working energies. For Zernike phase contrast system, the intensity downstream of the sample is given by[21]

$$\begin{aligned} I_\mathrm{s} \;=\; & A_0A_0^*\{\mathrm{e}^{-\mu_2 t}(\mathrm{e}^{-\mu_\mathrm{p}t_\mathrm{p}}+1)+\mathrm{e}^{-\mu_\mathrm{s}t} \\ & +2\mathrm{e}^{-\mu_\mathrm{s}t/2}\mathrm{e}^{-\mu_\mathrm{b}t/2}\mathrm{e}^{-\mu_\mathrm{p}t_\mathrm{p}/2}\cos[(\eta_\mathrm{s}-\eta_\mathrm{b})t-\eta_\mathrm{p}t_\mathrm{p}] \\ & -2\mathrm{e}^{-\mu_\mathrm{s}t/2}\mathrm{e}^{-\mu_\mathrm{b}t/2}\cos[(\eta_\mathrm{s}-\eta_\mathrm{b})t] \\ & -2\mathrm{e}^{-\mu_\mathrm{b}t}\mathrm{e}^{-\mu_\mathrm{p}t_\mathrm{p}/2}\cos(\eta_\mathrm{p}t_\mathrm{p})\}, \end{aligned} \tag{3}$$

and the intensity of the image of the matrix (background) is

$$I_\mathrm{b} = A_0A_0^*\mathrm{e}^{-\mu_\mathrm{b}t}\mathrm{e}^{-\mu_\mathrm{p}t_\mathrm{p}}, \tag{4}$$

where A_0 is the complex amplitude on the incident plane, μ_s, μ_b, and μ_p are the absorption coefficients of sample, matrix, and phase ring, respectively, η_s, η_b, and η_p are the phase shift coefficients, t is the thickness of the sample, and t_p the thickness of the phase ring.

3. Results

In order to show the performance improvement in terms of the dose, we calculate the PND ratio: $n_r = \mathrm{PND(absorption)/PND(phase)}$. The model consists of a small Zn particle in a 5-μm cell. Working energies for the calculation are 1022.3 eV and 973.7 eV, 1022.3 eV and 992.9 eV, 1022.3 eV, and 1012.4 eV for the phase contrast and 1022.3 eV and 1012.4 eV for the absorption. The variations of PND ratio with nanoparticle size are shown in Fig. 4 correspondingly. Taking 20-nm Zn particle for example, the PND ratio of the absorption contrast imaging to phase contrast imaging can be up to 4.3, which means that dose can be reduced down to $\sim 1/4$ that with the absorption method. We should also notice that the required exposure for the new method decreases as the difference between the two energies increases. This is because the difference in phase shift increases as one energy moves away from the absorption edge. However, this is not the case in the absorption method, thus we can further optimize the results by broadening the energy spacing in a certain range.

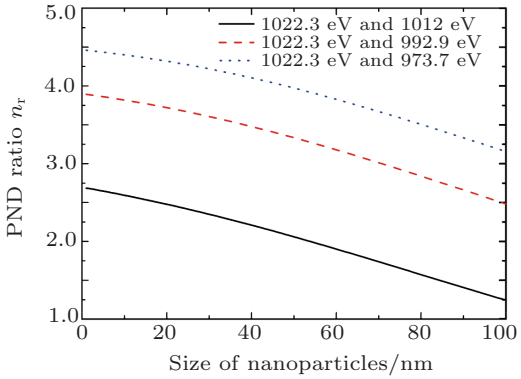


Fig. 4. (color online) Performance improvement in terms of exposure. The variations of ratio of the required x-ray exposure (PND) in absorption contrast to that in phase contrast with the size of the nanoparticles. Energies for absorption are 1022.3 eV and 1012.4 eV, and energies for phase contrast are indicated in the upper right corner of the figure.

We also perform similar calculations for other metals such as Cu, Fe, and Ti, data based on Ref. [4]. Results indicate that for small size particles (< 100 nm), elemental imaging based on the phase contrast is more efficient, i.e., at constant SNR the PND for phase contrast is halved or even quartered compared with that in the absorption method.

In addition, we evaluate the performance of the new method in terms of the size of the particles, and the results show that our phase contrast technique is always more effective than the absorption method, as long as the object particle size is smaller than 100 nm. Our new method is suitable for the soft x-ray range. Also, we should mention that the data from Ref. [4] are not exactly accurate near absorption edges, but for metals they are close to the realistic ones. Since no molecular orbitals are involved, we will consider these situations in our following work.

4. Conclusions

Our proposed elemental x-ray phase contrast imaging method exploits the intrinsic phase changes of resonance peaks, which enables us to achieve low dose element-specific x-ray imaging. Despite several limitations, this new imaging method can be used in a wide range of biological applications, such as three-dimensional (3D) imaging of metal protein clusters, and even in material sciences, such as transition process of metal clusters in battery materials. Finally, our proposed method can serve as a good complement to XANES imaging and XFM techniques, and easily implement with current TXM microscopes.

References

[1] Engstrom A 1946 *Acta Radiol. Suppl.* **63** 7
[2] Kennedy J M, Jacobsen C, Kirz J, Rarback H, Cinotti F, Thomlinson W, Rosser R and Schidlovsky G 1985 *J. Microsc-Oxford* **138** 321
[3] Henke B L, Gullikson E M and Davis J C 1993 *Atom. Data Nucl. Data* **54** 181
[4] http://henke.lbl.gov/optical_constants/

[5] Klems J H 1991 *Phys. Rev. A* **43** 2041

[6] Bernhard P, Maul J, Berg T, Wegelin F, Ott U, Sudek C, Spiecker H, Merchel S and Schonhense G 2006 *Phys. Rev. B* **74** 075401

[7] Grew K N, Chu Y S, Yi J, Peracchio A A, Izzo J R, Hwu Y, Carlo F D, and Chiu W K S 2010 *J. Electrochem. Soc.* **157** B783

[8] Yin G C, Tang M T, Song Y F, Chen F R, Liang K S, Duewer F W, Yun W, Ko C H and Shieh H D 2006 *Appl. Phys. Lett.* **88** 241115

[9] Fan J D and Jiang H D 2012 *Acta Phys. Sin.* **61** 218702 (in Chinese)

[10] Sun L, Huo Y, Zhou C, Liang J H, Zhang X Z, Xu Z J, Wang Y and Wu Y Z 2015 *Acta Phys. Sin.* **64** 197502 (in Chinese)

[11] Chen J, Gao K, Wang Z L, Yun W B and Wu Z Y 2015 *Chin. Phys. B* **24** 086804

[12] Zhang K, Li D E, Hong Y L, Zhu P P, Yuan Q X, Huang W X, Gao K, Zhou H Z and Wu Z Y 2013 *Chin. Phys. B* **22** 076801

[13] Shahzad F, Siddiqi S A, Im M Y, Avallone A, Fischer P, Hussain Z, Siddiqi I and Hellman F 2010 *Chin. Phys. B* **19** 037504

[14] Chen Y T, Chen T Y, Yi J, Chu Y S, Lee W K, Wang C L, Kempson I M, Hwu Y, Gajdosik V and Margaritondo G 2011 *Opt. Lett.* **36** 1269

[15] Schneider G 1998 *Ultramicroscopy* **75** 85

[16] Schmahl G, Rudolph D, Guttmann P, Schneider G, Thieme J and Niemann B 1995 *Rev. Sci. Instrum.* **66** 1282

[17] Zhang K, Li D E, Hong Y L, Zhu P P, Yuan Q X, Huang W X, Gao K, Zhou H Z and Wu Z Y 2013 *Chin. Phys. B* **22** 076801

[18] Liu Y J, Meirer F, Wang J Y, Requena G, Williams P, Nelson J, Mehta A, Andrews J C and Pianetta P 2012 *Anal. Bioanal. Chem.* **404** 1297

[19] Wang Z L, Gao K, Chen J, Hong Y L, Ge X, Wang D J, Pan Z Y, Zhu P P, Yun W B, Jacobsen C and Wu Z Y 2013 *Biotechnol. Adv.* **31** 387

[20] London R A, Rosen M D and Trebes J E 1989 *Appl. Opt.* **28** 3397

[21] Duke P J and Michette A G 1990 *Modern Microscopies – Techniques and Applications* (New York: Springer) p. 59